Assessment of groundwater metals contamination using geoelectric methods and pollution index around nickel mine Pomalaa District, Kolaka Regency, Southeast Sulawesi

Nur Robithotul Sugiono[1], *Ferryati* Masitoh[1*], *Denis* Mararis[2], Kurniawan[2]

[1] Department of Geography, State University of Malang, Malang Regency, Indonesia
[2] PT. Indra Karya (Persero) Survey and Investigation Division, Malang Regency, Indonesia

Abstract. Nickel mining operations can significantly impact groundwater quality by releasing metallic contaminants. This study aims to quantify metal concentrations in groundwater quality changes at nickel mining sites in Pomalaa District, Kolaka Regency. The study employs the Wenner configuration geoelectric technique and Pollution Index (IP) to assess metal pollution in groundwater. Geoelectric data, log borings, laboratory results of groundwater quality, and regional geological maps were used in the study. Water sample analysis detected toxic elements such as Aluminum, Iron, Manganese, Zinc, Copper, Hexavalent Chromium, Nickel, Cobalt, Cadmium, and Lead. Geoelectric analysis shows that groundwater is generally found within fracture zones of igneous and metamorphic rocks at depths between 2 and 100 meters. The Pollution Index (IP) categorized the groundwater samples as moderately contaminated, failing to meet drinking water quality standards. The analysis suggests that the groundwater originates from fissures in ultramafic rock, with significant metal contamination detected in groundwater wells. Metal content in groundwater occurs due to the interaction between rocks and groundwater. The study results also show that the groundwater pollution index is in the light category. However, the levels of heavy metals mean that groundwater cannot be directly used to fulfill needs. Further processing of groundwater is necessary so that groundwater can be used.

1 Introduction

The Southeast Sulawesi Province possesses significant potential in nickel commodities, with an estimated reserve of 97.4 billion tons distributed across a land area of 480 thousand hectares [1]. Pomalaa district located in the western part of Southeast Sulawesi, is known for its abundant nickel deposits. These deposits are valuable minerals that contain metal oxides with high concentrations of nickel (Ni) and iron (Fe) [2–4]. These resources help to establish many nickel mines in the Pomalaa district.

Nickel ore mining activities can significantly contribute to environmental contamination [5,6]. Heavy metals can contaminate groundwater [7,8]. Geological analysis uses geoelectric theory to assess the vertical and horizontal arrangement of geological formations. This theory is based on studying the electrical conductivity of water to determine potential difference values [9].

The Pollution Index approach was used to evaluate the extent of water pollution in the groundwater quality analysis [10]. The results analysis reveals the specific parameters responsible for poor water quality, enabling the implementation of appropriate pollution management strategies. The approach was selected due to its ability to examine individual data, resulting in efficient time and cost for establishing water quality conditions. In contrast, other methods, like the STORET method, necessitate time series data [11].

The aims of this study are: 1) identify the geological conditions; 2) identify the pollution index classes of heavy metals; and 3) evaluate the impact of heavy metal pollution on groundwater users in the region. The objective of this paper is to present new insights into metal contamination in groundwater by employing geoelectric methods and pollution indices that have not been previously documented in the literature. Previous studies have only utilized pollution indices [12][13], to discuss the impact of geology on groundwater and surface water quality in the Pomalaa district mine area. This study will provide additional information on the lithology and heavy metal pollution in the Pomalaa district.

2 Method

2.1. Research location

The study was conducted in a nickel mine area with a geographic coordinate of 4˚10'42" S - 4˚15'10" S and 121˚38'3" E - 121˚41'6" E. Nickel mine located in Pomalaa sub-district, Kolaka district, Southeast Sulawesi province (Fig. 1). Pomalaa district is at an altitude of 380

* Corresponding author: ferryati.masitoh.fis@um.ac.id

meters which has a varied terrain [3,14]. The study was conducted in the Pomalaa district. Subsequently, the Survey and Investigation Division of PT Indra Karya (Persero) Office was used for data processing, interpretation analysis, and report writing. The data collection period extended from January 2021 to January 2024.

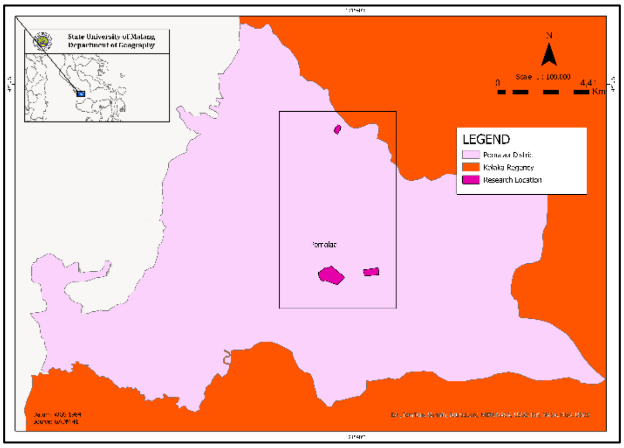

Fig. 1. Research Location (Based on [15] modified).

2.2. Acquisition data

The research process consists of four stages, which are illustrated in Fig. 2. The first, preparatory stage, begins with an investigation related to the research to be carried out. During this stage, the problem topic and research objectives are determined, followed by a literature study relevant to the subject and objectives. In the second stage, collect data, which is categorized into primary and secondary data sources. The primary data includes groundwater quality test data from 8 groundwater samples, processed drill log data from three sources, and geoelectric data from 5 passes. Additionally, the secondary data consists of a regional geological map of the Kolaka sheet obtained through the Ministry of Energy and Mineral Resources of the Republic of Indonesia website.

During the data collection stage, activities are carried out to gather the necessary data. In the process of groundwater sampling within the nickel mining area, employ a random sampling method from 8 groundwater wells to ensure comprehensive coverage. The number of samples collected is determined to provide an accurate representation of the area's groundwater conditions. These samples were then analyzed in the laboratory to obtain the levels of water quality parameters.

The collection of drill log data was successfully performed at specific points along the geoelectric track, including lines B, C, and E. This data was obtained at depths ranging from 128 to 203 meters, determined by the saturation of the rock profile. The Wenner alpha configuration method was used because of its superior sensitivity in detecting lateral and shallow changes compared to other electrode configurations. The Wenner-Alpha configuration consists of four electrodes, including two current and two potential electrodes arranged in a straight line Fig. 3. The location of the geo-electrical prospecting route considering mining activities (see Fig. 1) (see in Fig. 4).

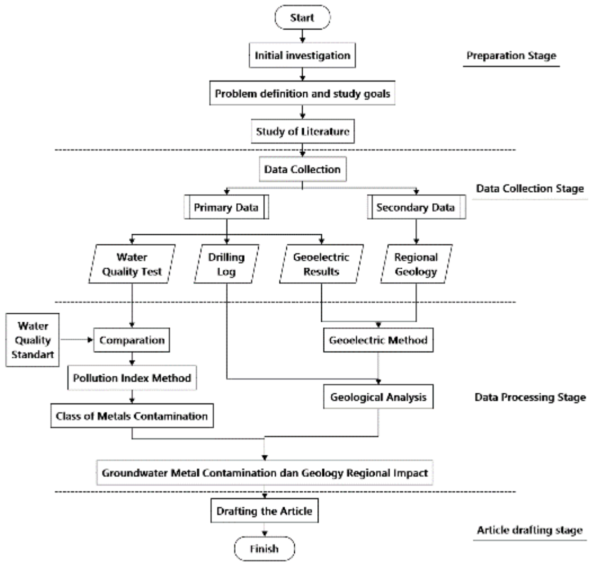

Fig. 2. Research flow chart.

Data and analysis were carried out in the third stage. The geoelectric data processing calculated apparent resistivity values, obtained through the apparent resistivity formula and geometry factor [16]. Subsequently, we will utilize Res2Dinv software to generate a 2D resistivity distribution image [17]. Lastly, finalize the process by drafting an article. The comparison of these results with established lithology and water resistivity tables [18,19] was used to discern the constituent lithology and to identify the type of water present in the area.

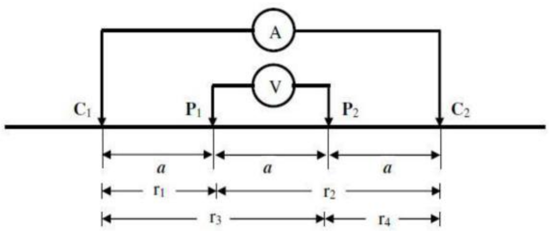

Fig. 3. Wenner-Alpha Configuration Model [18].

The resistivity obtained through the geoelectric method reflects the apparent resistivity (ρ), which is determined using the apparent resistivity equation (1) and geometric correction (2) [20]. This technique serves as an effective approach for analyzing the horizontal variations in the specific resistance of subsurface layers [21]. The apparent specific gravity value is calculated based on the assumption that the Earth is an isotropic homogeneous medium, and it is formulated as follows:

$$\rho_\alpha = k\frac{\Delta V}{I} \tag{1}$$

With k is a geometric factor of Wenner α configuration

$$k = 2\pi\, a \tag{2}$$

ρ_α is apparent resistivity (Ωm); ΔV is potential (mV); I is the current injected into the earth (*I*); and *k* is the geometric factor, where *a* is electrode spacing (m).

Further data processing by comparing the interpretation results with [18,19]. The interpretation results describe lithology and water type based on the appropriate resistivity value range. The analysis involved verifying the interpretation results using regional geological data and logs to improve accuracy.

The analysis of water quality test data will involve comparing it to the drinking water quality standards outlined in Regulation of the Minister of Health no. 2 (2023). This regulation sets forth the safe limits of dissolved content in water for consumption, as chosen by the author. This new regulation is known for its innovative approach and has garnered recognition. By comparing the obtained values, we can pinpoint variations in each element, which will enable us to calculate the pollution index effectively.

The Pollution Index approach is utilized to assess the level of pollution to water quality standards (BMA) based on heavy metals parameters [23,24]. The IP approach assesses pollution levels using both an average index to provide an overview and a maximum index to identify the most influential parameter (2). To assess water quality status, we will use the average result from the index, as specified in Permen LH No. 115 (2003) regulations.[10].

According to these regulations, an IP score ranging from 0 to 1.0 is classified as Good Condition, an IP score ranging from >1.0 to 5.0 is classified as Lightly Polluted, an IP score ranging from >5.0 to 10 is classified as Moderately Polluted, and an IP score greater than 10 is classified as Heave Polluted. Equation (3) calculates the PI value using the formula [25]:

$$the\ PI = \sqrt{\frac{(Ci/Lij)^2_{Maks} + (Ci/Lij)^2_R}{2}} \tag{3}$$

PI is the pollution index value; Ci is the concentration of measured; Li is the quality standard for the concentration; Max is the highest value of concentration; and R is the average value of concentration.

3 Result and discussion

3.1 Regional geology of the study area

The Pomalaa district is part of three distinct geological formations, as outlined in the Regional Geological Map of Kolaka Sheet [26] (Fig. 4): Ultramafic Complex (Ku): Comprising harzburgites, dunite, wherlit, serpentinite, garbo, basalt, dolerite, diorite, metamafic, amphibolite, magnesite, and local rodingite. This formation originated during the limestone period. Langkowala Formation (Tml): Consists of conglomerate, sandstone, shale, and occasional calcarenite. The conglomerate contains quartz, quartzite, malih sandstone, schist, and ultrabasic rocks and dates back to the Miocene epoch. Alangga Formation (Qpa): Comprising conglomerate and sandstone were deposited in an inland brackish environment during the Pleistocene.

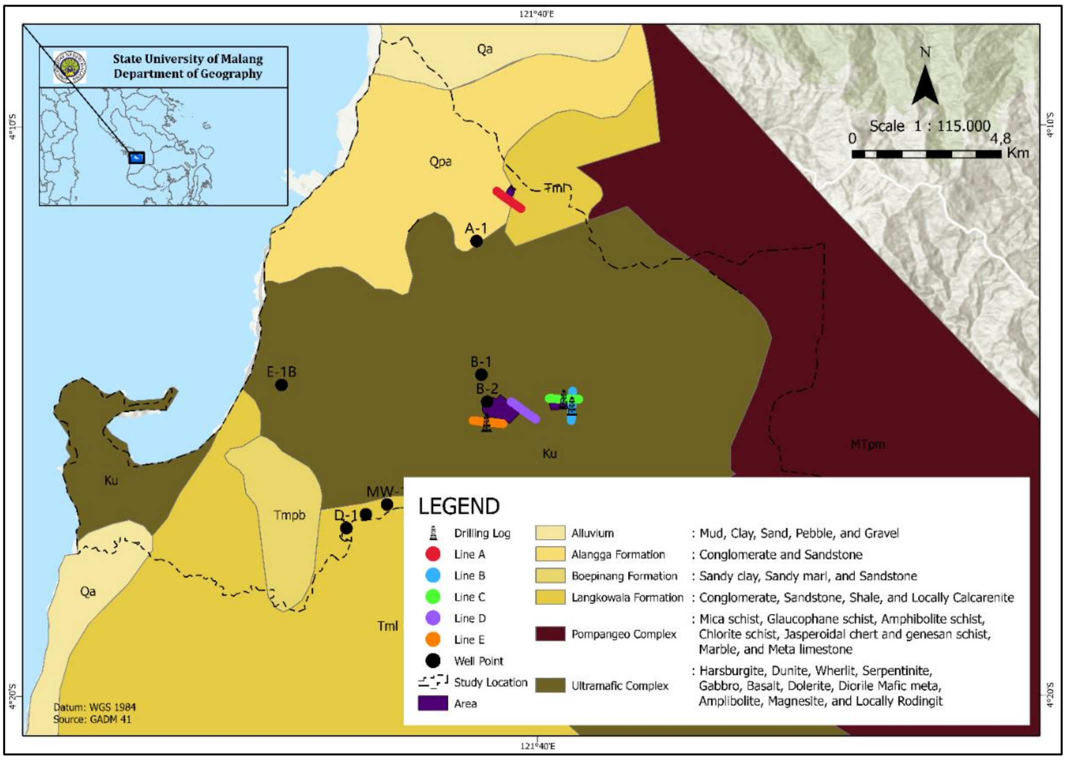

Fig. 4. Regional Geological Map of the Study Area (sources from [15] modified).

3.2 Geoelectric Investigation Results

The resistivity data was acquired using the Wenner configuration geoelectric method, employing a fixed electrode distance of 21 meters. To meet the data requirements, the electrode spacing has been calculated to cover a length of 987 meters, allowing for data collection to a depth of 200 meters. Field data collection was conducted along five lines, and the line locations were classified into two distinct areas: the Alangga-Langkowala area and the Ultramafic Complex area. These classifications were adapted to the geological formations passed through.

In the Alangga-Langkowala area, there is a line A that extends from the northwest (A1) to the southeast (A2). The line is 987 meters long and has a penetration depth of 130 meters. Line A is situated within the Alangga and Langkowala Formations Fig. 4. The resistivity measurements yielded a range of resistivity values from 5.40 Ωm to 9635 Ωm, with an RMS error of 29.4%. After analyzing the resistivity processing, the RMS error obtained shows how much confidence the data processing results have. The RMS error value is adjusted based on the configuration and geological formation of the research site areas the RMS error tolerance can be less than 30% [27].

Based on the resistivity tables by [18,19], the following interpretations can be made resistivity values between 4 and 9 Ωm indicate a soil object and values falling within the range of 10 Ωm to 100 Ωm typically correspond to the presence of groundwater objects. Values exceeding 100 Ωm and ranging up to 9635 Ωm generally denote sedimentary rocks with lower porosity levels, such as sandstone, shale, limestone, and conglomerate. Groundwater can typically be found at depths ranging from 3 to 70 meters, with the specific depth determined by the type of lithology, which indicates a depressed aquifer show in **Fig. 5**.

Following the analysis of resistivity processing and validation through the application of the V law principle in structural geography and geological regional mapping, it has been determined that the area under survey consists of four distinct layers. Of particular note, two of these layers correspond to the intersecting boundaries between different geological formations. The geological survey indicates that two layers exhibit sandstone lithology with differing porosity variations, while the lower layer demonstrates the presence of conglomerate, which possesses greater porosity and higher resistivity values ranging from 1134 to 9631 Ωm. The lithological examination of the study area reveals the presence of conglomerate and sandstone.

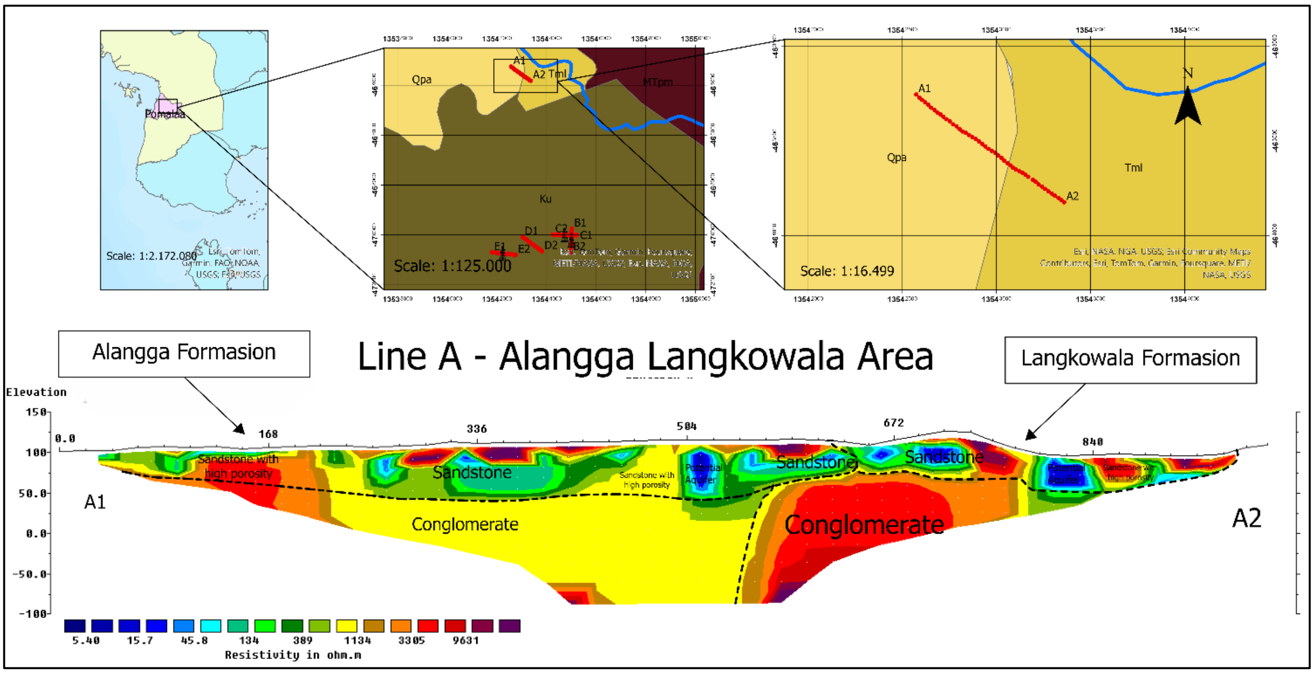

Fig. 5. Cross-section Interpretation of Line A.

Line A is located in Ground Water Basin Kolaka, which is characterized by a free aquifer consisting of sedimentary rocks, including limestone and sandstone. The aquifer has a thickness ranging from 10 to 60 meters. The permeability and porosity characteristics of rocks will influence groundwater recharge [28]. However, an anomaly was found in the form of a high resistivity value in the upper layer, which may be caused by the presence of deposits in the form of highly porous sandstone.

In the Ultramafic Complex area, measurements were made on four lines, namely the intersecting B-C line and the parallel D-E line. The lines are located within the Ultramafic Complex (Ku) but outside the Groundwater Basin Unit **Fig. 4**. The measured resistivity values ranged from 5.40 Ωm to 9635 Ωm, with an RMS error of 28.2-36.1%. Based on resistivity tables by [18,19], the interpretation is that resistivity values between 4 and 9 Ωm indicate the presence of soil, and values in the range of 10 Ωm to 100 Ωm indicate the presence of groundwater. Values exceeding 100 Ωm and ranging up to 9635 Ωm indicate sedimentary, igneous, and metamorphic rocks with varying degrees of porosity,

 https://doi.org/10.1051/bioconf/202414601038

such as sandstones, schists, basalt, and gabbro. Groundwater is found at depths ranging from 3 to 80 meters, with lithological types indicating fractured aquifers as shown in **Fig. 6**. After analyzing the resistivity processing, the RMS error obtained shows how much confidence the data processing results have. The RMS error value is adjusted based on the configuration and geological formation of the research site, for complex ultramafic areas the RMS error tolerance can be less than 30% [27,29].

In examining the interpretation results, we combined three key datasets: interpretation results, drill log data, and regional geological data. Our analysis reveals the presence of olivine, pyroxene, and amphibole as the main mineral compositions.

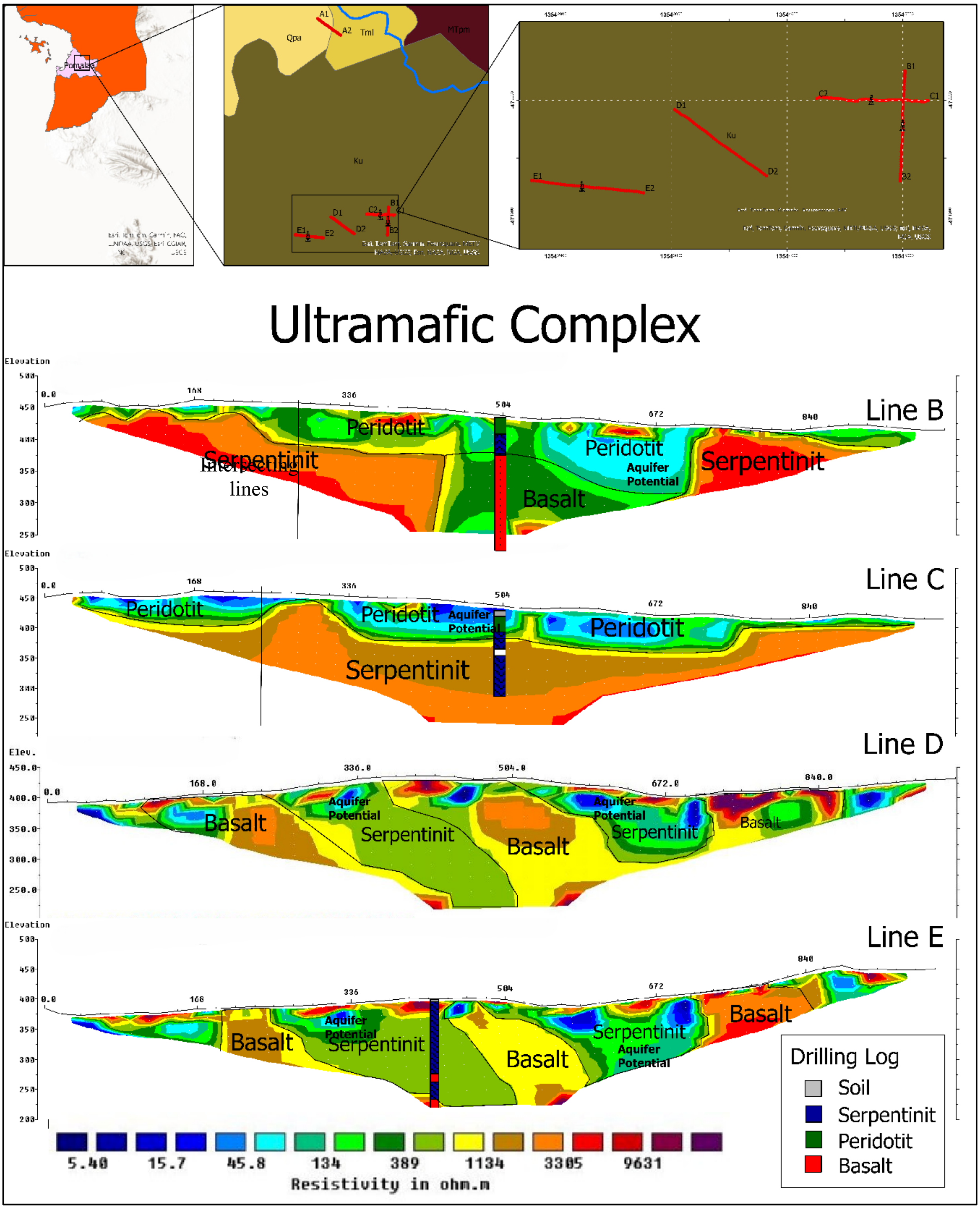

Fig. 6. Cross-section Interpretation of Lines B-C and D-E.

The drill log data indicates that the lithology consists of Peridotite, Serpentinite, and Basalt. **Fig. 4** in the regional geological data illustrates the various lithologies in the Ultramafic Complex, including harsburgite, dunite, wherlit, serpentinite, garbo, and basalt. Furthermore, harsburgite, dunite, and wherlit are lithologies derived from peridotite starting rocks [26]. As a result, based on the validation of the processing results, the lithology on the BCDE track comprises peridotite (harsburgite, dunite, wherlit), serpentinite, and basalt.

The lithological boundary layers were determined by analyzing resistivity patterns from different passes. This process resulted in a more accurate analysis and interpretation of the data (**Fig. 6**). On the B - C line, an intersecting layer pattern was observed, with the upper layer composed of peridotite and serpentinite, and a depressed aquifer found within. The lower layer consisted mainly of serpentinite with some basalt to the south. On the D - E line, an undulating pattern was detected, likely pushed from the east. The blue color on the map indicates the presence of groundwater-bearing strata with low resistivity values, estimated to be 10-80 meters thick. This zone is primarily composed of igneous and metamorphic rocks with low to extremely low permeability. It features a fractured aquifer system with varying groundwater potential, ranging from minor to relatively larger quantities, along with occasional discharge.

3.3 Groundwater metal content

The laboratory analysis of groundwater samples collected from 8 groundwater wells (including boreholes and monitoring wells) has revealed the presence of various metal chemical elements, namely pH, Aluminum (Al), Iron (Fe), Manganese (Mn), Zinc (Zn), Copper (Cu), Hexavalent Chromium (Cr-VI), Nickel (Ni), Cobalt (Co), Cadmium (Cd), and Lead (Pb) (**Fig. 7**). Due to inadequate data obtained, 16 metal element values were not recorded, along with one well. The water quality testing findings were subsequently calibrated according to the quality requirements outlined in Regulation of the Minister of Health No. 2 (2023) [30]. The comparison results indicate that there are multiple metrics, including metal components, that surpass the established quality criteria.

Based on the comparison results, it has been determined that the pH, Fe, Cd, Co, Cr-VI, Mn, and Pb levels exceed the water quality standards. Contamination levels of Al, Ni, Zn, and Cu remain below the established threshold. The analysis indicates that among the groundwater wells, the highest contamination levels are found in Co (5 wells), pH (2 wells), and Cd (1 well), while the lowest contamination levels are observed in Cu (4 wells), Mn (2 wells), pH (1 well), Pb (1 well), and Cd (1 well). The contamination levels at both the highest and lowest ends are below the threshold, indicating that there is no low content in each well. In the study area, the Cu contamination exhibits the lowest susceptibility to contamination. The predominant constituents in the groundwater composition include Co, exhibiting a high susceptibility to contamination, as well as pH and Cd. Although Fe, Cr-VI, Mn, and Pb do not represent the primary materials, they still necessitate treatment due to their lower susceptibility compared to pH and Cd.

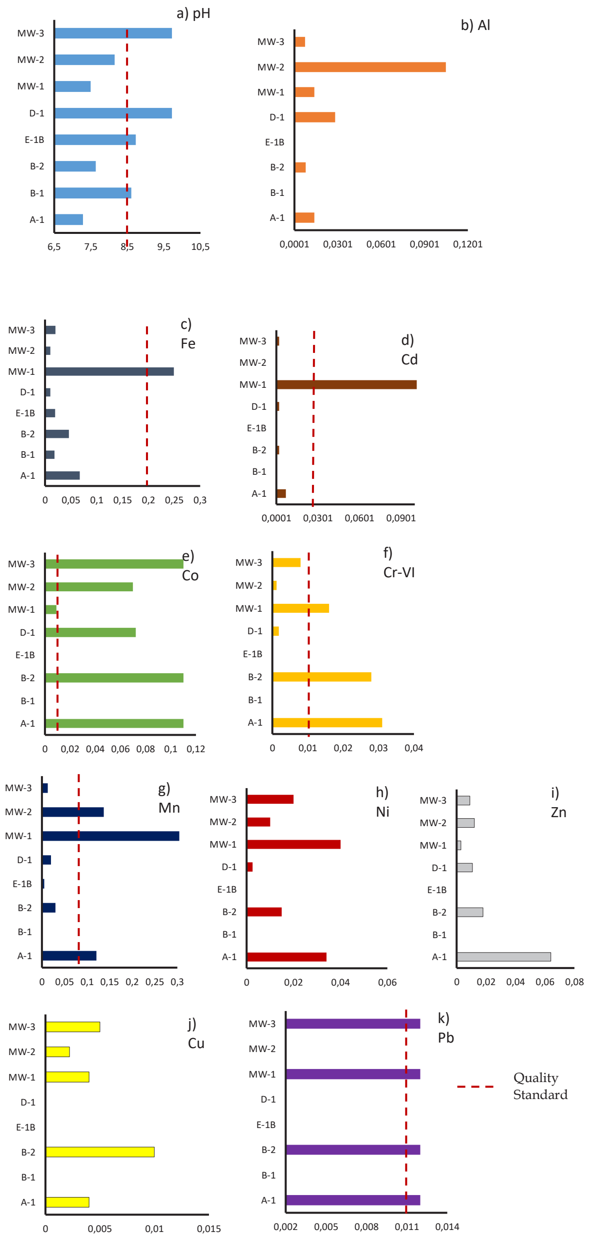

Fig. 7. In groundwater analysis, the following solutes were identified: a) Potential of Hydrogen (pH) - 4 wells exceeded the standard, b) Aluminum (Al) - no wells exceeded the limit, c) Iron (Fe) - 1 well exceeded the standard, d) Cadmium (Cd) - 1 well exceeded the standard, e) Cobalt (Co) - 5 wells exceeded the standard, f) Chromium (Cr-VI) - 3 wells exceeded the standard, g) Manganese (Mn) - 3 wells exceeded the standard, h) Nickel (Ni) - no wells exceeded the standard, i) Zinc (Zn) - no wells exceeded the standard, j) Copper (Cu) - no wells exceeded the standard, and k) Lead (Pb) - 4 wells exceeded the standard. This data is integral for informed decision-making and implementing appropriate measures to address the solute levels in the groundwater.

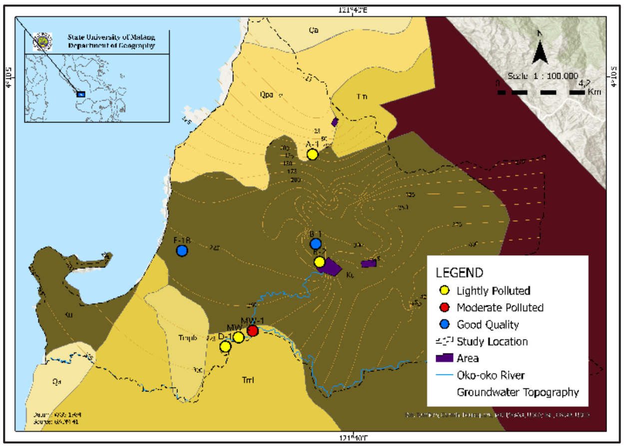

Fig. 8. Pollution level map.

The calculation of the IP (a) value indicates that the groundwater samples class is categorized into three sections by Regulation of the Minister of Health No. 115 (2003) Appendix II (Table 1) [10]. The average groundwater contamination level falls within the range of 3.7-4.5, which corresponds to class 2, indicating lightly polluted. Wells B-1 and E-1B have pollution levels with good quality scoring ≤1.0. On the other hand, well MW-1 is classified as moderately polluted, scoring 7.5 (Fig. 8).

Naturally, lithology has the greatest influence on groundwater quality, among many other factors. The porosity of the rock determines the openings through which rainwater penetrates. According to Steven et al. (2021), these pores enable the dissolution and storage of elements present in the rock [12]. Higher amounts of dissolved elements are found in rocks that have been occupied by groundwater for longer than that. Pratistho et al. (2018) found that the porosity value of the rock increases as the number of fractures in it increases. The result of this influence is an increased risk of pollution in compact rocks with more fractures [31].

3.4 Impact of metals in groundwater

According to the geoelectric identification results, the study area is composed of two lithologies: the ultramafic complex with peridotite lithology and the Alangga-Langkowala with conglomerate lithology (Fig. 6, Fig. 6). The Ultramafic Complex geology is composed of olivine, pyroxene, and amphibole [12,32]. Semi-metallic and metallic elements are derived from constituent minerals, including Fe, Ni, and Al [14,33,34]. The elements that exceed the standard on the pollution index are pH, Co, Cr-VI, and Pb (Fig. 7). High pH values can be the result of the weathering of ultramafic rocks, which releases Fe and Mg into the groundwater. The mineral content in groundwater can be influenced by products from mining around the well, resulting in a content of Co, Cr-VI, and Pb that exceeds the quality standards.

Minerals in the Alangga and Langkowala geologies are composed of sandstone and conglomerate fragments. Lithic peridotite with a medium-sized matrix and silica cement are the lithologic constituent fragments [12]. The elements that exceed the standard on the pollution index are pH, Fe, Cd, Co, Cr-VI, Mn, and Pb. The elements Co, Cd, and Pb are at risk of contamination due to mining activities. High Fe contamination is influenced by lithological conditions that have Fe elements, especially in Ultramafic lithology. Oxidation of the lithology causes Fe to increase and Cu and Al minerals to decrease [35]. Potential mineral dissolution from constituent fragments, which produces high pH values by dissolving Fe elements. As anthropogenic pollution comes closer, the pH value in the well increases due to the low groundwater elevation. Higher-elevation wells have an alkaline pH, which is influenced by lithology, while lower-elevation wells have a neutral pH (Fig. 8).

As a result of the velocity and distribution of groundwater flow, porous media are more susceptible to pollution [36,37]. In the research area, the peridotite lithology is dispersed, and the pollution index value is quite high due to the porous character of the laterite soil, which readily absorbs water. The conglomerate lithology with the highest pollution index exhibits a value difference that is influenced by the overlying peridotite lithology and is indicative of the influence of lower groundwater contours Fig. 8 [38]. In the hydrological cycle, groundwater flows naturally due to variations in soil layer elevation and pressure [39,40]. Contaminants will move with the groundwater flow and ultimately reach the well if the well is situated at the lower portion of the pollution source location.

Natural lithological factors have the greatest impact on groundwater quality, as precipitation dissolves substances in the rock as it passes through its fissures [41]. Rainwater, which is influenced by the porosity of the granite, penetrates through the fissures with variable intensity over time . The level of solute content increases as the duration of groundwater's occupancy of a rock increases [13]. Groundwater bonds an increased number of chemical elements as a consequence of the ions present in the contacted solid minerals [42]. Increased ion binding results in a decline in groundwater quality.

The literature study explained that lithological contact affects groundwater quality, but the findings showed that industrial activity factors bring a lot of variation in metal contamination. Groundwater ions in contact with lithology bind rock chemistry, which is generally major ions. Heavy metals in contact with groundwater are rarely found in large quantities. Nickel mining activities cause groundwater contamination through surface water entering the groundwater cycle. River water that carries metal elements can be the cause of high Pb content.

The use of contaminated groundwater, especially in wells with mild and moderate pollution indices, may pose health risks [43]. Groundwater treatment is necessary to be able to utilize groundwater in life Remediation technologies for soils and groundwater [44]. The continued presence of metal contamination in groundwater causes a complete breakdown of the groundwater cycle if not resolved. Groundwater purification and remediation can be one way to reduce metal contamination in groundwater [45].

4 Conclusion

Geoelectric identification has revealed the presence of ultramafic and metamorphic rocks, along with some conglomerate rocks. The mineral composition includes iron (Fe), magnesium (Mg), nickel (Ni), and aluminum (Al). The pollution index categorizes the groundwater into three levels: satisfying the standard, lightly contaminated, and moderately polluted. Wells classified as having a moderate pollution index contains elevated levels of cadmium, which can be harmful to the organ and reproductive systems if ingested. The groundwater is found in a fractured aquifer composed of ultramafic and partially sedimentary rocks. Test wells indicate minor contamination with metallic elements, though the groundwater generally shows low levels of pollution. Despite the generally minor contamination, regular consumption of this groundwater could pose health risks due to cadmium. Therefore, it is essential to treat the water before use to ensure safety. It is recommended to implement appropriate water treatment measures to remove contaminants, particularly cadmium, in order to ensure safe drinking water. Future studies should focus on long-term monitoring of groundwater quality and the effectiveness of different water treatment technologies to address potential contamination issues.

References

1. M. H. Suharjo, R. Ernawati, and Nurkhamim, J. Pendidik. Tambusai **6**, 11978 (2022)
2. R. Raivel and F. Firman, J. GEOMining Tek. Pertamb. Unkhair, **2**, 11 (2022)
3. H. Kamaruddin, R. A. I.K., M. F. Rosana, N. Sulaksana, and E. T. Y, Bul. Sumber Daya Geol. **13**, 84 (2018)
4. C. Helvacı, T. Oyman, İ. Gündoğan, H. Sözbilir, O. Parlak, S. Kadir, and N. Güven, Can. J. Earth Sci. **55**, 252 (2018)
5. M. S. Agussalim, A. Ariana, and R. Saleh, Palita J. Soc. Relig. Res. **8**, 37 (2023)
6. C. Asdak, *Hidrologi Dan Pengelolaan Daerah Aliran Sungai* (UMG PRESS, 2023)
7. A. A. I. S. Yusuf, in *Semin. Nas. Teknol. Ind.* (2021), pp. 358–361
8. T. K. Boateng, F. Opoku, and O. Akoto, Appl. Water Sci. **9**, 1 (2019)
9. F. R. Allan and J. A. Cherry, *Groundwater* (Prentice Hall-Internationl Inc, Englewood Cliffs, New Jersey, 1979)
10. Kementerian Negara Lingkungan Hidup, *Keputusan Menteri Negara Lingkungkan Hidup No. 115 Tentang Pedoman Penentuan Status Mutu Air* (2003)
11. Machairiyah, Z. Nasution, and B. Slamet, LIMNOTEK Perair. Darat Trop. Di Indones. **27**, 13 (2020)
12. S. Steven, M. Muliddin, and A. Okto, OPHIOLITE J. Geol. Terap. **3**, 9 (2021)
13. A. Rubaiyn, A. Okto, Jahidin, La Ode Sahiddin, La ode Andimbara, and S. Asfar, J. Rekayasa Geofis. Indones. **5**, 1 (2023)
14. Hasria, Masri, M. A. Azzaman, and M. Jerniawan, J. Geosci. Eng. Environ. Technol. **8**, 10 (2023)
15. T. O. Simanjuntak, Surono, and Sukido, *Peta Geologi Lembar Kolaka* (Pusat Penelitian dan Pengembangan Geologi, Bandung, 2011)
16. A. S. Akingboye and A. C. Ogunyele, Rud. Geol. Naft. Zb. **34**, 93 (2019)
17. Jamaluddin and E. P. Umar, IOP Conf. Ser. Earth Environ. Sci. **118**, (2018)
18. W. M. Telford, L. P. Geldart, and R. E. Sheriff, *Applied Geophysics*, Second Edi (Cambridge University Press, Cambridge, 1990)
19. Loke M. H., *Electrical Imaging Surveys for Environmental and Engineering Studies: A Practical Quide to 2-D and 3-D Surveys.* (1999)
20. M. Juandi and E. N. Ginting, J. Phys. Conf. Ser. **2049**, (2021)
21. Z. Erwanto, A. Afandi, N. R. P, and M. D. Tirto, Pros. SNITT-Politeknik Negeri Balikpapan **1**, 1 (2017)
22. Djoko Santoso, *Pengantar Teknik Geofisika* (Penerbit ITB, Bandung, 2002)
23. M. Aristawidya, Z. Hasan, Iskandar, Yustiawati, and H. Herawati, LIMNOTEK Perair. Darat Trop. Di Indones. **27**, 27 (2020)
24. D. Marganingrum, D. Roosmin, Pradono, and A. Sabar, J. Ris. Geol. Dan Pertamb. **23**, 37 (2013)
25. Nelson L. Nemerow, *Benefits of Water Quality Enhancement*, Volume 161 (Environmental Protection Agency, Water Quality Office, 1970)
26. A. Kadarusman, S. Miyashita, S. Maruyama, C. D. Parkinson, and A. Ishikawa, Tectonophysics **392**, 55 (2004)
27. R. Alpiandi, Identifikasi Sebaran Bijih Besi Di Bawah Permukaan Menggunakan Metode Electrical Resistivity Dan Induced Polarization Di Nangabulik, Kalimantan Tengah, Universitas Islam Negeri Syarif Hidayatullah, 2021
28. F. BÖRNER, M. GRUHNE, and J. SCHÖN, Geophys. Prospect. **41**, 83 (1993)
29. H. Pazha, M. Nasro, and R. Denya Agustina, J. Phys. Conf. Ser. **1175**, (2019)
30. Menteri Kesehatan RI, *Peraturan Menteri Kesehatan Republik Indonesia Nomor 2 Tentang Peraturan Pelaksanaan Peraturan Pemerintah Nomor 66 Tahun 2014 Tentang Kesehatan Lingkungan* (2023), pp. 29–34
31. B. Prastistho, P. Pratiknyo, C. Prasetyadi, M. R. Massora, and Y. K. Munandar, *Hubungan Struktur Geologi Dan Sistem Air Tanah*, 1st ed. (LPPM UPN “Yogyakarta” Press, Yogyakarta, 2018)
32. J. F. Lewis, Contrib. to Mineral. Petrol. **38**, 197

(1973)

33. C. R. L. Friend, V. C. Bennett, and A. P. Nutman, Contrib. to Mineral. Petrol. **143**, 71 (2002)
34. W. L. Griffin, S. R. Shee, C. G. Ryan, T. T. Win, and B. A. Wyatt, Contrib Miner. Pet. **134**, 232 (1999)
35. A. Neaman, J. Chorover, and S. L. Brantley, Am. J. Sci. **305**, 147 (2005)
36. M. O. Ofomola, B. D. Ako, and A. O. Adelusi, Arab. J. Geosci. **9**, (2016)
37. D. S. MacFarlane, J. A. Cherry, R. W. Gillham, and E. A. Sudicky, J. Hydrol. **63**, 1 (1983)
38. K. Martínek and K. Štolfová, Bull. Geosci. **84**, 555 (2009)
39. D. F. Bradford, K. Stanley, L. L. McConnell, N. G. Tallent-Halsell, M. S. Nash, and S. M. Simonich, Environ. Toxicol. Chem. **29**, 1056 (2010)
40. G. L. Daly and F. Wania, Environ. Sci. Technol. **39**, 385 (2005)
41. M. Sakizadeh and E. Ahmadpour, Environ. Earth Sci. **75**, 1 (2016)
42. I. A. Abboud, Environ. Geochem. Health **40**, 1405 (2017)
43. V. M. Wagh, D. B. Panaskar, S. V. Mukate, S. K. Gaikwad, A. A. Muley, and A. M. Varade, Model. Earth Syst. Environ. **4**, 969 (2018)
44. A. Bhandari, R. Y. Surampalli, P. Champagne, S. K. Ong, R. D. Tyagi, and I. M. C. Lo, Remediat. Technol. Soils Groundw. **60**, 1 (2007)
45. M. A. Hashim, S. Mukhopadhyay, J. N. Sahu, and B. Sengupta, J. Environ. Manage. **92**, 2355 (2011)